Proceedings of the 2007 American Control Conference
Marriott Marquis Hotel at Times Square
New York City, USA, July 11-13, 2007



# Design and Analysis of an Activator-Repressor Clock in *E. Coli*

D. Del Vecchio

*Abstract*— **We analyze a model for the activator-repressor oscillator motif proposed as a fundamental oscillating motif in the literature of biological rhythms. We show that incorporating the m-RNA dynamics in the model, we can obtain a much richer dynamical behavior with respect to the behaviors observed in the literature when only protein dynamics were modeled. The proposed analysis also leads to biochemical parameter relationships that guarantee stable oscillations. These relationships can be used as design guidelines for the construction of synthetic activator-repressor oscillators.**

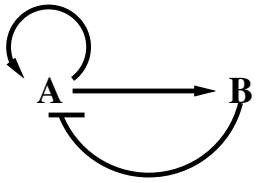


Fig. 1. Activator-repressor oscillator motif.

## I. I

Oscillations play a fundamental role in cell physiology. The cell cycle in which cells periodically duplicate their genome and divide is an important oscillator [11]. Another example is the circadian clock, a very robust and accurate biochemical circuit that produces oscillations with the period of one day. This particular clock is also a remarkable example of an adaptive system, which can be entrained to follow daily variations such as temperature and light. Genetic oscillator motifs based on the interaction of a small set of molecular components have been shown to appear recurrently in the regulation of the cell cycle [1]. In particular, oscillator motifs involving an autocatalytic element competing with a repressor have been shown to play a key role in the regulation of the cell cycle of the *Xenopus laevis* embryos [10]. Thus, synthetic biologists have attempted to understand the properties of a small circuit motif composed of a composite negative feedback loop and a positive autoactivation loop (see Figure 1), by constructing an instance of it to be tested in isolation [2]. We will refer to this oscillator motif as activator-repressor oscillator.

In this paper, we consider an instance of such a motif in which the repression occurs through transcriptional regulation and we propose two different models: a two-dimensional ordinary differential equation model and a four-dimensional ordinary differential equation model. In the two-dimensional model, the m-RNA dynamics are neglected as they are considered to be faster than the protein dynamics. These m-RNA dynamics are instead explicitly considered in the four-dimensional model. The objective of our analysis is to determine the range of dynamical behaviors of the two models of the proposed topology when the biochemical parameters are varied. On the one hand, the results of this analysis can be employed to guide the design and fabrication of a synthetic clock *in vivo*. On the other hand, the obtained results are useful to establish whether the proposed oscillator motif and related models are descriptive enough to capture phenomena that are experimentally observed in natural clocks and whether previously unseen behaviors can be predicted.

The activator-repressor topology here considered, has been already modeled by a second order model neglecting the m-RNA dynamics in [6]. In such a work, the authors conclude that oscillations appear only when a clear separation of time-scales between the activator and the repressor dynamics is present. In this paper, we show that this requirement is not needed if the m-RNA dynamics are also modeled. For the four-dimensional model, we show that a stable limit cycle appears any time the separation of time-scales between the activator and the repressor reaches a threshold value, which can be close to one, and which depends on the speed of the m-RNA dynamics. Such a threshold value is determined by a Hopf bifurcation, which is supercritical when the m-RNA dynamics is sufficiently fast compared to the protein dynamics and subcritical when protein and m-RNA dynamics evolve on comparable time-scales.

In this paper, we also show that the four-dimensional model exhibits a transition from simple to complex oscillatory behavior [5], which has not been recorded before. This transition occurs as the separation of time scales between the protein and the m-RNA dynamics decreases, and thus as the four-dimensional model becomes far apart from the two-dimensional one. In particular, two types of complex oscillatory behaviors are found: (a) the coexistence of a stable equilibrium point and a stable periodic orbit (*hard excitation* situation [8]) and (b) the coexistence of two stable periodic orbits (*birhythmicity* [4]). The birhythmicity phenomenon does not appear to be practically relevant as the parameter range in which two stable orbits coexist is so small to be numerically impossible to set a parameter value inside it. The hard excitation situation occurs for small time-scale separation between m-RNA dynamics and protein dynamics and for parameter values that are numerically appreciable. This phenomenon is practically relevant especially because it has been shown to be the potential cause of circadian rhythm suppression [8]. In fact, in presence of a stable equilibrium point and of a stable periodic orbit, small external perturbations (such as light) can cause the system to move into the

1-4244-0989-6/07/$25.00 ©2007 IEEE.

basin of attraction of the stable equilibrium point. The system will thus stop oscillating until a new perturbation appears that will move the system back in the region of attraction of the periodic orbit.

Finally, by confronting our parametric analysis with the experimental data provided in [2], which shows almost sinusoidal damped oscillations, we can obtain a qualitative understanding of where the biochemical parameters of the system in [2] lie in parameter space.

This paper is organized as follows. In Section II, we introduce the system and the fourth order dynamical model. In Section III, we determine the range of dynamical behaviors for the case in which the system admits one equilibrium point only. By using bifurcation analysis, two key parameters are varied: the time-scale difference between the activator and the repressor and the time-scale difference between the protein and m-RNA dynamics. In Section IV, we determine conditions on all the biochemical parameters that guarantee the existence of a unique equilibrium point. Finally, for the two-dimensional model, we determine analytic sufficient conditions for the existence of a stable periodic orbit.

## II. A F - D M

Consider the activator-repressor diagram shown in Figure 1. Let $r_A$ and $r_B$ represent the concentration of m-RNA of the activator and of the repressor, respectively. Let $A$ and $B$ denote the protein concentration of the activator and of the repressor, respectively. Then, we consider the following four-dimensional model describing the rate of change of the species concentrations:

$$\begin{aligned} \dot{r}_A &= -\delta_1/\epsilon\, r_A + F_1(A,B) \\ \dot{A} &= \nu(-\delta_A A + k_1/\epsilon\, r_A) \\ \dot{r}_B &= -\delta_2/\epsilon\, r_B + F_2(A) \\ \dot{B} &= -\delta_B B + k_2/\epsilon\, r_B, \end{aligned} \tag{1}$$

in which the parameter $\nu$ regulates the difference of time-scales between the repressor and the activator dynamics, $\epsilon$ is a parameter that regulates the difference of time-scales between the m-RNA and the protein dynamics. The parameter $\epsilon$ determines how close the model (1) is to a two-dimensional model in which the m-RNA dynamics are considered at the equilibrium. Thus, $\epsilon$ is a singular perturbation parameter. Model (1) is not exactly in singular perturbation form. To take it to singular perturbation form, one can consider the change of variables $\overline{r}_A = r_A/\epsilon$ and $\overline{r}_B = r_B/\epsilon$, so that model (1) becomes

$$\begin{aligned} \epsilon\dot{\overline{r}}_A &= -\delta_1\, \overline{r}_A + F_1(A,B) \\ \dot{A} &= \nu(-\delta_A A + k_1\, \overline{r}_A) \\ \epsilon\dot{\overline{r}}_B &= -\delta_2\, \overline{r}_B + F_2(A) \\ \dot{B} &= -\delta_B B + k_2\, \overline{r}_B. \end{aligned} \tag{2}$$

We choose to consider the form (1) for performing parametric analysis because for system (2) the Floquet exponents [7] of the periodic orbits are very small so that there are numerical problems when trying to determine the stability of the periodic orbits. The functions $F_1$ and $F_2$ are the Hill functions as, for example, found in [1]. These are given by

$$F_1(A,B) = \frac{K_1 A^n + K_{A0}}{1 + \gamma_1 A^n + \gamma_2 B^n} \text{ and } F_2(A) = \frac{K_2 A^n + K_{B0}}{1 + \gamma_4 A^n},$$

in which $K_1$ and $K_2$ are the maximal transcription rates, while $K_{A0}$ and $K_{B0}$ are the maximal transcription rates when no activator is present. The parameters $1/\gamma_i$ are the activation coefficients and are related to the affinity of the protein to the promoter site. The Hill coefficient $n$ is chosen here to be $n = 2$. A justification of this choice can be found in Section IV.

The system can have 1, 3, and 5 equilibria. The values of $\epsilon$ and of $\nu$ do not affect the number of equilibria, while the values of the other parameters are the ones that control this number. The set of values of $K_i, k_i, \delta_i, \gamma_i, \delta_A, \delta_B$ that allow the existence of a unique equilibrium is determined in Section IV. In the sequel, we assume that the values of $K_i, k_i, \delta_i, \gamma_i, \delta_A, \delta_B$ have been chosen so that there is a unique equilibrium and we study the occurrence of periodic solutions as the difference in time-scales between protein and m-RNA, $\epsilon$, and the difference in time-scales between activator and repressor, $\nu$, are changed.

## III. B A F - M

In this section, the values of $K_i, k_i, \delta_i, \gamma_i, \delta_A, \delta_B$ are set to constant values that guarantee that the system has a unique equilibrium. The specific values that we consider are $\delta_A = \delta_B = 1$, $K_1 = K_2 = 4 * 10^4$, $\delta_1 = \delta_2 = 1$, $k_1 = k_2 = 0.01$, $K_{A0} = 4$, $K_{B0} = 0.4$. The range of dynamical behaviors is explored by using bifurcation analysis as $\nu$ and $\epsilon$ are changed.

We let $1/\epsilon$ vary in the range $[1, 1000]$, in which, $\epsilon = 1$ corresponds to equal time-scales for protein and m-RNA dynamics, while $1/\epsilon = 1000$ corresponds to large separation of time-scales between protein and m-RNA dynamics. For $1/\epsilon = 1000$, the system in equations (1) behaves as a two-dimensional system in which the first and the third equations in (1) are considered at the equilibrium.

For each value of $1/\epsilon$, we performed a bifurcation analysis with bifurcation parameter $\nu$. By computing the linearization of the system at its unique equilibrium, we varied $\nu$ and determined that a Hopf bifurcation occurs. In fact, as $\nu$ increases over a threshold value, two of the eigenvalues of the linearization cross the imaginary axis, while the other two eigenvalues maintain negative real parts. We then computed the Floquet exponent of the periodic orbit originating from Hopf bifurcation by using the algorithm suggested in [7]. If the Floquet exponent is negative, the periodic orbit is stable and a supercritical Hopf bifurcation occurs. If the Floquet exponent is positive, the periodic orbit is unstable and the Hopf bifurcation is subcritical. We summarize in Table I our

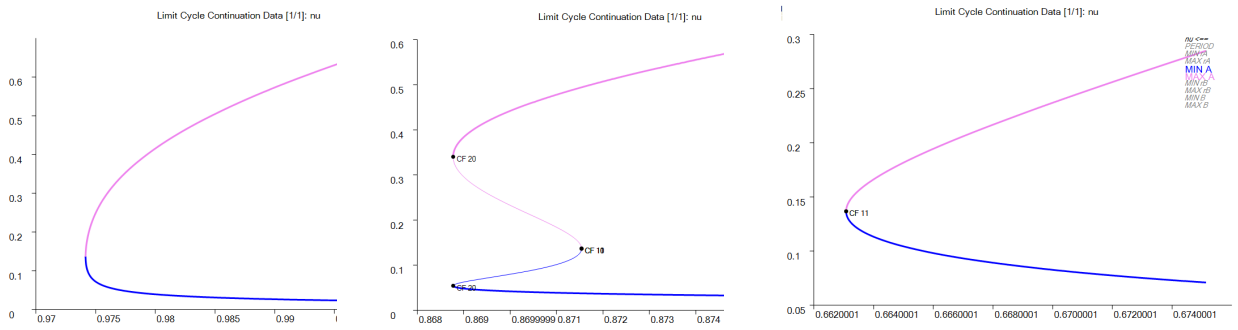


Fig. 2. In each diagram, the horizontal axis corresponds to the value of $\nu$. The vertical axis indicates the amplitude of the periodic orbit. The magenta trait corresponds to the maximal amplitude, while the blue trait corresponds to the minimal amplitude. The tick line denotes a stable orbit, while the thin line denotes an unstable orbit. The left-side plot is representative of diagrams occurring for $\epsilon^{-1} > 100$ (in particular, it corresponds to $\epsilon^{-1} = 150$) and Hopf bifurcation occurs for $\nu = 0.974$. The plot in the middle is representative of diagrams occurring for $20 \leq \epsilon^{-1} \leq 100$ (in particular, it corresponds to $\epsilon^{-1} = 50$) and Hopf bifurcation occurs for $\nu = 0.9092$. The right-side plot is representative of diagrams occurring for $\epsilon^{-1} < 20$ (in particular, it corresponds to $\epsilon^{-1} = 10$) and Hopf bifurcation occurs for $\nu = 0.6637$. The acronym CF denotes cyclic fold bifurcation.

findings.

Table I

| $\epsilon^{-1}$ | $\nu^*$ | $\beta_2$ | Hopf Bifurcation |
|---|---|---|---|
| 1000 | 1.00635 | $-1.28 * 10^3$ | supercritical |
| 800 | 1.00635 | −814.85 | supercritical |
| 600 | 1.003 | −448.51 | supercritical |
| 400 | 0.998 | −191.72 | supercritical |
| 300 | 0.9930 | −103.86 | supercritical |
| 200 | 0.9838 | −43.02 | supercritical |
| 100 | 0.9573 | −8.85 | supercritical |
| 90 | 0.9518 | −6.87 | supercritical |
| 70 | 0.936 | −3.69 | supercritical |
| 50 | 0.9092 | −1.51 | supercritical |
| 20 | 0.7939 | −0.0321 | supercritical |
| 10 | 0.6637 | +0.05 | subcritical |
| 1 | 0.2466 | +0.0014 | subcritical |

In Table I, $\nu^*$ denotes the value of $\nu$ at which a Hopf bifurcation occurs for the values of $\epsilon$ specified in the first column. From the table, we note that a stable limit cycle arises from Hopf bifurcation (supercritical case) for sufficient separation of time-scales between the m-RNA and the protein dynamics. When this separation of time scales is not large enough the periodic orbit originating from Hopf bifurcation is unstable (subcritical case). Despite this result, numerical simulation with Matlab did not show a small amplitude sinusoidal limit cycle for $\epsilon^{-1} \in [20, 100]$ even for values of $\nu - \nu^*$ of the order of $10^{-14}$. Only large amplitude relaxation-type oscillations were exhibited. To clarify this point, we computed bifurcation diagrams using AUTO continuation software [3] with $\nu$ as bifurcation parameter for the values of $\epsilon^{-1} \in [1, 1000]$. The continuation of the periodic orbit arising at the Hopf bifurcation gives rise to fundamentally three types of diagrams depending on the range of $\epsilon^{-1}$ values. These are shown in Figure 2. From the left-side plot of Figure 2 ($\epsilon^{-1} > 100$), we deduce that a supercritical Hopf bifurcation is the only bifurcation involving the periodic orbit. This agrees with Table I and with simulation results showing a small amplitude almost sinusoidal limit cycle for values of $\nu$ close to the bifurcation value. The plot in the middle and the right-side plot show cyclic fold bifurcations. Cyclic fold bifurcations are saddle nodes of periodic orbits [9] and occur when an unstable orbit crashes against a stable one and they disappear. The cyclic fold bifurcations CF10 and CF11 occur so close to the Hopf bifurcation of the equilibrium point, that AUTO was unable to distinguish between them and the Hopf bifurcation.

By Table I, we know that almost in correspondence of CF10 there is a supercritical Hopf bifurcation and almost in correspondence of CF11 there is a subcritical Hopf bifurcation. Taking this in formation into account, the qualitative bifurcation diagrams corresponding to the cases in Figure 2 can be drawn as in Figure 3. In the middle plot of Figure 3 ($20 \leq \epsilon^{-1} \leq 100$), the values of $\nu$ at which Hopf bifurcation occurs and at which the cyclic fold bifurcation CF10 occurs are so close that it is numerically impossible to pick a value of $\nu$ between them. Therefore, the small sinusoidal orbit arising from Hopf bifurcation, even if stable, will never be observed in simulation or in the biological setting. Instead, only large amplitude relaxation oscillations originating from the cyclic fold bifurcation C20 will be observed. This phenomenon occurs because a saddle node bifurcation of the periodic orbit occurs extremely close to a supercritical Hopf bifurcation. A similar phenomenon is also present for $\epsilon^{-1} < 20$, in which a cyclic fold bifurcation CF11 is extremely close to a subcritical Hopf bifurcation. In this case, a small amplitude almost sinusoidal limit cycle is observed in simulation, despite the Hopf bifurcation is subcritical, because the cyclic fold bifurcation is very close to the Hopf bifurcation point. In the middle plot of Figure

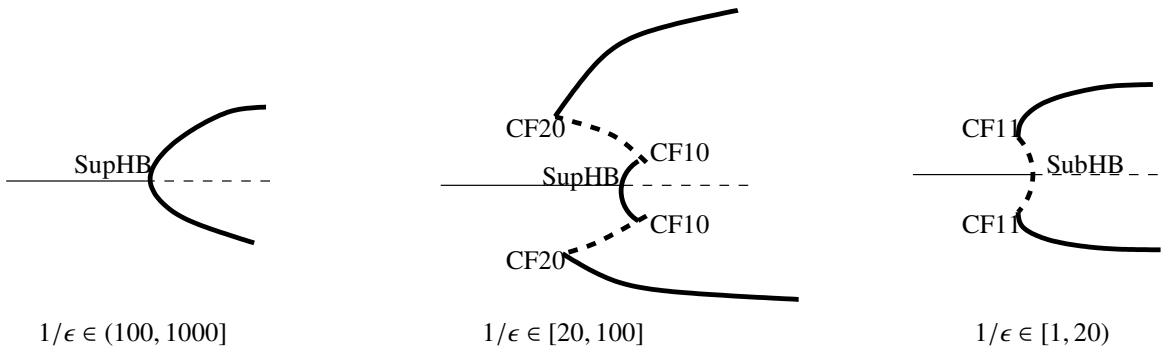


Fig. 3. Bifurcation diagrams with $\nu$ (on the horizontal axis) as bifurcation parameter as $\epsilon^{-1}$ changes in the specified intervals. The amplitude of $A$ is displayed. Solid lines denote stable equilibrium points, while dashed lines denote unstable equilibrium points. Solid thick lines denote the amplitude of a stable periodic orbit, while dashed thick lines denote the amplitude of an unstable periodic solution. The upper branches denote the largest amplitude, while the lower branches denote the smallest amplitude of the periodic orbit. SupHB denotes a supercritical Hopf bifurcation, SubHB denotes a subcritical Hopf bifurcation, and CF denotes a cyclic fold bifurcation.

3, we notice that there are values of $\nu$ for which a stable equilibrium point and a stable orbit coexist and values of $\nu$ for which two stable orbits coexist. The interval of $\nu$ values for which two stable orbits coexist is too small to be able to numerically set $\nu$ in such an interval. Thus, this interval is not practically relevant. The values of $\nu$ for which a stable equilibrium and a stable periodic orbit coexist is instead relevant. This situation corresponds to the *hard excitation* condition and occurs for realistic values of the separation of time-scales between protein and m-RNA dynamics. Therefore, this simple oscillator motif described by a four-dimensional model can capture the features that lead to the long term suppression of circadian rhythms by external inputs. *Birhythmicity* is also possible even if practically not relevant due to the numerical difficulty of moving the system to one of the two periodic orbits. More investigation is required to determine what features of the system cause a cyclic fold bifurcation to occur at almost the same value of a Hopf bifurcation. This would also shed light into what features may lead the system to exhibit practically relevant birhythmicity.

All of these results are summarized by Figure 4. According to this figure, the region of the parameter space in which the system exhibits almost sinusoidal damped oscillations is on the left-hand side of the curve corresponding to the Hopf bifurcation. Therefore, the data of [2] may correspond to a system whose operating parameters are such that $\nu$ is on the "left" of the curve corresponding to the Hopf bifurcation. As a consequence, increasing the separation of time-scales between the activator and the repressor, $\nu$, should lead to a stable relaxation-type large amplitude limit cycle.

## IV. A T - M

In this section, we consider the limit for $\epsilon \to 0$ in equations (2) and consider the resulting second order model:

$$\begin{aligned} \dot{A} &= \nu(-\delta_A A + f_1(A,B)) \\ \dot{B} &= -\delta_B B + f_2(A), \end{aligned} \tag{3}$$

in which $f_1(A,B) = (k_1/\delta_1)F_1(A,B)$ and $f_2(A) = (k_2/\delta_2)F_2(A)$. We next establish parameter conditions for which we can guarantee that there is a unique equilibrium and that it is unstable and not locally a saddle. Thus, by Poincarè-Bendixson Theorem we can infer that for such a parameter set, the $\omega$-limit set of the system is a periodic orbit.

### *A. Conditions for the existence of a unique and unstable equilibrium*

Let $\bar{K}_1 = K_1(k_1/(\delta_1\delta_A))$, $\bar{K}_{A0} = K_{A0}(k_1/(\delta_1\delta_A))$, $\bar{K}_2 = K_2(k_2/(\delta_2\delta_B))$, $\bar{K}_{B0} = K_{B0}(k_2/(\delta_2\delta_B))$ and let

$$f(A,B) := \nu(-\delta_A A + f_1(A,B)) \text{ and } g(A,B) := -\delta_B B + f_2(A). \tag{4}$$

Then, the nullcines are given by $f(A,B) = 0$ and $g(A,B) = 0$, which define $B$ as a function of $A$ in the following way:

$$f(A,B) = 0 \quad \Longrightarrow \quad B = \left(\frac{\bar{K}_1 A^n + \bar{K}_{A0} - A(1+\gamma_1 A^n)}{\gamma_2 A}\right)^{1/n} \tag{5}$$

$$g(A,B) = 0 \quad \Longrightarrow \quad B = \frac{\bar{K}_2 A^n + \bar{K}_{B0}}{1+\gamma_3 A^n}, \tag{6}$$

where the Hill coefficient $n$ is a variable parameter.

**Proposition 1:** If $n = 1$, system (3) admits a unique stable equilibrium point. If $n = 2$, system (3) admits a unique equilibrium point if the following parameter relations are verified

$$0 < \bar{K}_{A0} \leq \frac{\bar{K}_1^3}{27\gamma_1^2},\ M \leq \frac{\bar{K}_2 A_M^2 + \bar{K}_{B0}}{1+\gamma_3 A_M^2},\ m \geq \frac{\bar{K}_2 A_m^2 + \bar{K}_{B0}}{1+\gamma_3 A_m^2}, \tag{7}$$

in which

$$\begin{aligned} A_m &= \frac{\bar{K}_1}{6\gamma_1}\left(1 - (cos(\phi/3) - \sqrt{3}sin(\phi/3))\right) \\ A_M &= \frac{\bar{K}_1}{6\gamma_1} + \frac{\bar{K}_1}{3\gamma_1}cos(\phi/3) \\ \phi &= \text{atan}\left(\frac{\sqrt{\frac{27\bar{K}_{A0}}{4\gamma_1^2}(\frac{\bar{K}_1^3}{\gamma_1^2} - 27\bar{K}_{A0})}}{\frac{\bar{K}_1^3}{4\gamma_1^3} - 27\frac{\bar{K}_{A0}}{2\gamma_1}}\right), \end{aligned} \tag{8}$$

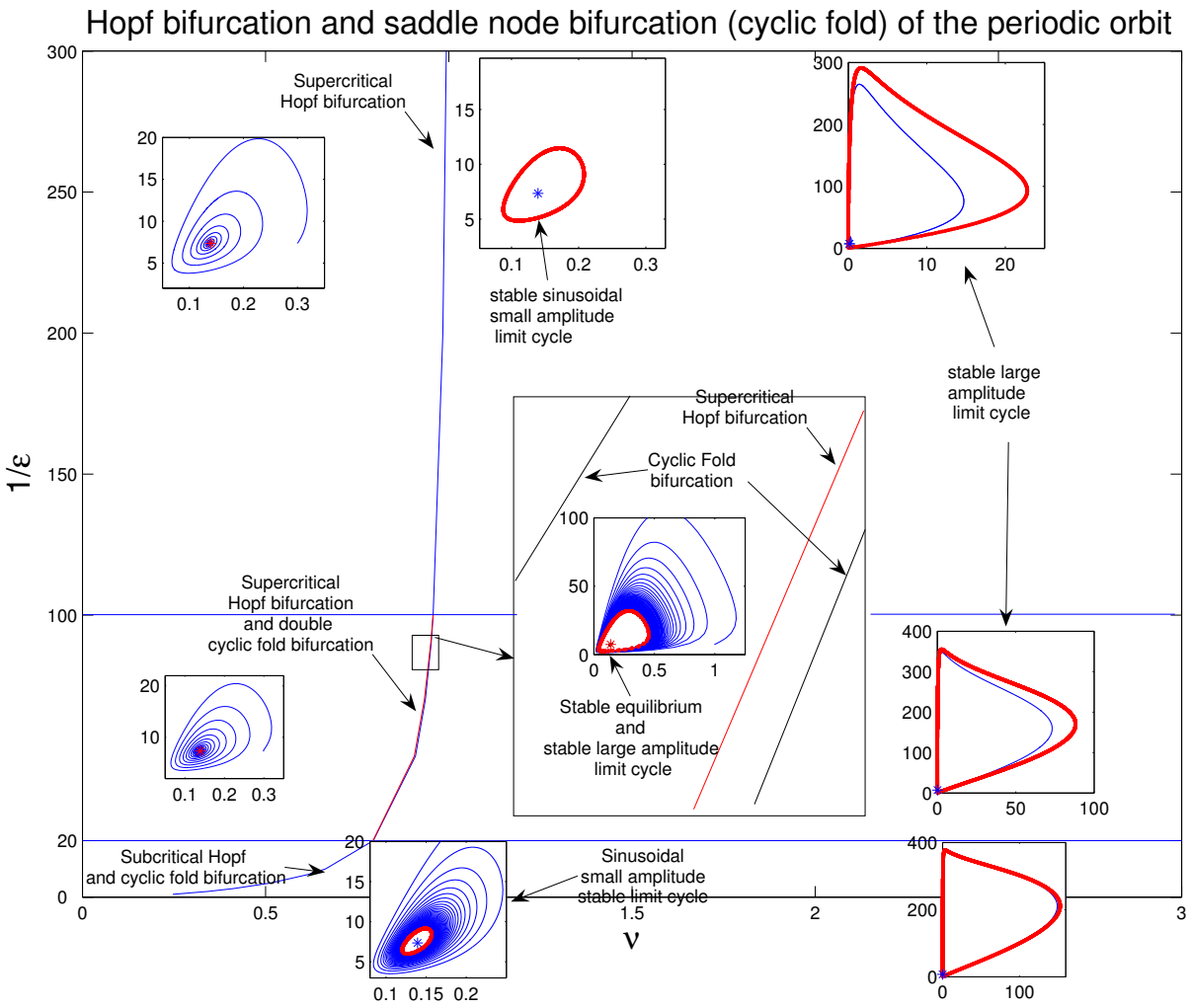


Fig. 4. Range of dynamical behaviors as the parameters $\epsilon^{-1}$ and $\nu$ are varied. The trajectories in the plots are the projections in the $A, B$ plane.

$$m = \sqrt{\frac{\bar{K}_1 A_m^2 + \bar{K}_{A0} - A_m(1+\gamma_1 A_m^2)}{\gamma_2 A_m}},$$

$$M = \sqrt{\frac{\bar{K}_1 A_M^2 + \bar{K}_{A0} - A_M(1+\gamma_1 A_M^2)}{\gamma_2 A_M}}.$$

For $n = 2$, the unique equilibrium point is unstable (not a saddle) if

$$\nu \geq \frac{\delta_B}{\frac{\partial f_1}{\partial A}|_S - \delta_A}. \tag{9}$$

*Proof:* We consider the linearized system of (3) at the equilibrium $S$. The linear approximation at $S$ is given by the matrix

$$JF(S) = \begin{pmatrix} \frac{\partial f}{\partial A} & \frac{\partial f}{\partial B} \\ \frac{\partial g}{\partial A} & \frac{\partial g}{\partial B}, \end{pmatrix},$$

in which the partial derivatives are computed at the equilibrium $S$. For an unstable node or spiral to occur, it is sufficient that

$$(i)\ \text{trace}(JF(S)) > 0, \text{ and } (ii)\ \det(JF(S)) > 0.$$

*Case 1:* $n = 1$. The nullcline $f(A, B) = 0$ has always negative slope, and therefore we always have only one equilibrium. We next show that such an equilibrium is always stable. Expression (5) with $n = 1$ leads to

$$\frac{dB}{dA}|_{f(A,B)=0} = \frac{-\gamma_1\gamma_2 A^2 - \bar{K}_{A0}\gamma_2}{(\gamma_2 A)^2} < 0.$$

Since $dB/dA|_{f(A,B)=0} = -(\partial f/\partial A)/(\partial f/\partial B)$ by the implicit function theorem and since $\partial f/\partial B < 0$, it must be that $\partial f/\partial A < 0$. As a consequence, $\text{trace}(JF(S)) < 0$ because $\frac{\partial g}{\partial B} = -\delta_B < 0$. To show that both eigenvalues of $JF(S)$ are negative, we are left to show that $\det(JF(S)) > 0$. This is readily seen to be true as we have that

$$\frac{dB}{dA}|_{g(A,B)=0} = -\frac{\partial g/\partial A}{\partial g/\partial B} > \frac{dB}{dA}|_{f(A,B)=0} = -\frac{\partial f/\partial A}{\partial f/\partial B} < 0,$$

thus implying that $\frac{\partial f}{\partial A}\frac{\partial g}{\partial B} - \frac{\partial f}{\partial B}\frac{\partial g}{\partial A} = \det(JF(S)) > 0$.

*Case 2:* $n = 2$. Figure 5 shows the only possible configuration of the nullclines in which (a) we have a unique equilibrium and (b) the nullclines are intersecting with the

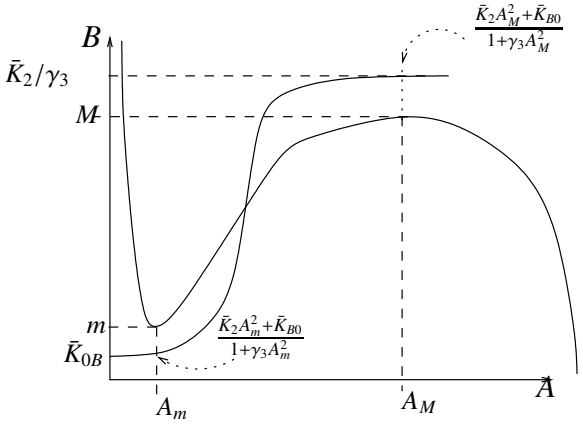


Fig. 5. Nullclines and the values $A_M$, $A_m$, $M$, and $m$.

same positive slope. The plots imply that

$$\frac{dB}{dA}|_{g(A,B)=0} = -\frac{\partial g/\partial A}{\partial g/\partial B} > \frac{dB}{dA}|_{f(A,B)=0} = -\frac{\partial f/\partial A}{\partial f/\partial B} > 0,$$

and thus that $\frac{\partial f}{\partial A}\frac{\partial g}{\partial B} - \frac{\partial f}{\partial B}\frac{\partial g}{\partial A} = \det(JF(S)) > 0$. By relations (4), we have that $\partial g/\partial A = \partial f_2/\partial A$, $\partial g/\partial B = -\delta_B$, $\partial f/\partial A = \nu(-\delta_A + \partial f_1/\partial A)$, and $\partial f/\partial B = -|\partial f_1/\partial B|$. If at the equilibrium point $S$ the nullcline $f(A,B) = 0$ has negative slope, $S$ is stable, as we have shown for the case $n = 1$. Therefore, we examine what additional conditions should be enforced to guarantee that the equilibrium point is unstable when the nullclines intersect both with positive slopes. Since condition (ii) is verified by the condition that the nullclines cross with positive slopes, we are left to provide conditions for which (i) is also true. To have that $\text{trace}(JF(S)) > 0$, we require that $\nu(\frac{\partial f_1}{\partial A} - \delta_A) - \delta_B > 0$, which is verified if condition (9) holds.

We next determine sufficient conditions on the parameters for having one crossing and such that the slopes of the two nullclines at the crossing are both positive (and thus (ii) is verified). This is performed by simple geometric considerations. For this purpose, consider Figure 5. The values $A_m$ and $A_M$ of the location of the minimum and maximum of $f(A,B) = 0$ can be computed by computing the derivative with respect to $A$ of expression

$$B^2 = \frac{\bar{K}_1 A^2 + \bar{K}_{A0} - A(1+\gamma_1 A^2)}{\gamma_2 A}$$

obtained by (5) and equating it to zero, as the square root function is monotone. This way, we find a third order polynomial that has two positive roots if $0 < \bar{K}_{A0} \leq \frac{\bar{K}_1^3}{27\gamma_1^2}$, otherwise it has one positive and two complex roots. These roots are given by relations (8) and they are shown in Figure 5. Thus, by looking at the same figure, one deduces that if conditions (7) are satisfied, we have on equilibrium point only, and (ii) is verified. ■

Note that conditions (7) implicitly depend on $\delta_A$, $\delta_B$, $\delta_1$, and $\delta_2$. These conditions are imposed on the seven parameters $\bar{K}_1$, $\bar{K}_2$, $\bar{K}_{A0}$, $\bar{K}_{B0}$, $\gamma_1$, $\gamma_2$, and $\gamma_3$. Once values for these parameters are set, one can use condition (9) to determine the value of $\nu$. For having one equilibrium point only, we have to require that the activator transcription rate that is proportional to $\bar{K}_{A0}$, must be sufficiently smaller then the maximal expression rate of the activator, which is proportional to $\bar{K}_1$. Also, $\bar{K}_{A0}$ must be non-zero. Also, in case $\bar{K}_1 >> \bar{K}_{A0}$, one can verify that $A_M \approx \bar{K}_1/2\gamma_1$ and thus $M \approx \bar{K}_1/2\sqrt{\gamma_1\gamma_2}$. As a consequence, conditions (7) require also that if $\bar{K}_1/\gamma_1$ increases then so must do $\bar{K}_2/\gamma_3$. This qualitatively implies that the maximal expression rate of the repressor divided by its protein and m-RNA decay rates must be larger than he maximal expression rate of the activator divided by its protein and m-RNA decay rates. Finally, $A_m \approx 0$, and $m \approx \sqrt{\bar{K}_{A0}/\gamma_2 A_m}$. As a consequence, conditions (7) also imply that the smaller $\bar{K}_{A0}$ becomes, the smaller $\bar{K}_{B0}$ must be. Condition (9) requires that $\nu$ must be sufficiently large. This last requirement matches the results obtained in Section II, in which stable oscillations are predicted to appear every time $\nu$ becomes larger than the Hopf bifurcation value.

## V. C

We have presented the analysis of a two-dimensional and a four-dimensional model of an activator-repressor gene oscillator, which has been proposed to be a fundamental motif in natural biological clocks. We have shown that incorporating the m-RNA dynamics in the model, we can obtain richer dynamical behavior, which was not previously observed in the two-dimensional models proposed in the literature. The parameter space that leads to stable limit cycles results from the proposed analysis.

## VI. A

The author would like to thank Prof. Eduardo Sontag for important discussions on the stability of the periodic orbits originating from Hopf bifurcation.

## R

[1] U. Alon. *An Introduction to Systems Biology: Design Principles of Biological Circuits*. Chapman & Hall, 2006.
[2] M. R. Atkinson, M. A. Savageau, J. T. Meyers, and A. J. Ninfa. Development of genetic circuitry exhibiting toggle switch or oscillatory behavior in *Escherichia Coli*. *Cell*, pages 597–607, 2003.
[3] E.J. Doedel. Auto, a program for the automatic bifurcation analysis of autonomous systems. *Cong. Numer.*, pages 265–384, 1981.
[4] A. Goldbeter. *Biochemical Oscillations and Cellular Rhythms. The molecular basis of periodic and chaotic behaviour*. Cambridge University Press, 1996.
[5] A. Goldbeter. Computational approaches to cellular rhythms. *Nature*, 420:238–245, 2002.
[6] R. Guantes and J. Poyatos. Dynamical principles of two-component genetic oscillators. *PLOS Computational Biology*, 2:188–197, 2006.
[7] L. N. Howard. Nonlinear oscillations. *Lectures in Applied Mathematics*, pages 1–67, 1979.
[8] J-C. Leloup and A. Goldbeter. A molecular explanation for the long-term suppression of circadian rhythms by a single light pulse. *Am. J. Physiol. Regulatory Integrative Comp. Physiol.*, 280:1206–1212, 2001.
[9] L. Perko. *Differential Equations and Dynamical Systems*. Springer, 1996.
[10] J. R. Pomerening, E.D. Sontag, and J. E. Ferrell. Building a cell cycle oscillator: hysteresis and bistability in the activation of cdc2. *Nat Cell Biol*, 5(4):346–351, April 2003.
[11] J. J. Tyson, A. Csikasz-Nagy, and B. Novak. The dynamics of cell cycle regulation. *Bioessays*, pages 1095–1109, 2002.